Thermal analysis on the pyrolysis of Tetrabromobisphenol A (TBBPA) and –Electric Arc Furnace Dust Mixtures

Mohammad Al-Harahsheh[1*], Awni Al-Otoom[1], Muhannad Al-Jarrah[1], Mohammednoor Altarawneh[2], Sam Kingman[3]

[1*] *Chemical Engineering Department, Jordan University of Science and Technology, Irbid, 22110, Jordan*

**Corresponding author: msalharahsheh@just.edu.jo*

[2] *School of Engineering and Information Technology, Murdoch University, Murdoch, WA 6150, Australia*

[3] *Faculty of Engineering, University of Nottingham, Nottingham, NG7-2RD, UK*

Abstract

The pyrolysis of Tetrabromobisphenol A (TBBPA) mixed with Electric Arc Furnace Dust (EAFD) was studied using thermogravimetric analysis (TGA) and theoretically analysed using thermodynamic equilibrium calculations. Mixtures of both materials with varying TBBPA loads (1:1, and 1:3) were prepared and pyrolyzed in a nitrogen atmosphere under dynamic heating conditions at heating rates of 5 and 10 ^{0}C/min. The mixtures degraded through several steps including decomposition of TBBPA yielding mainly HBr, bromination of metal oxides, followed by their evaporation in the sequence of $CuBr_3$, $ZnBr_2$, $PbBr_2$, $FeBr_2$, $MnBr_2$, KBr, NaBr, $CaBr_2$ and $MgBr_2$, and finally reduction of the remaining metal oxides by the char formed from decomposition of TBBPA. Thermodynamic calculations suggest the possibility of selective bromination of zinc and lead followed by their evaporation leaving iron in its oxide form, while the char formed may serve as a reduction agent for iron oxides into metallic iron. However, at higher TBBPA volumes, iron bromide forms, which can be also evaporated at a temperature higher than those of $ZnBr_2$ and $PbBr_2$. Results from this work provide practical insight into

selective recovery of valuable metals from EAFD while at the same time recycling the hazardous bromine content in TBBPA.

Keywords: Tetrabromobisphenol A, Pyrolysis, Electric Arc Furnace Dust, Thermogravimetric Analysis, thermodynamic calculations

1. Introduction

Steel can be considered as the most recycled material with more than 650 Mt tonnes recycled annually [1]. According to the World Steel Association [1], Electric Arc Furnaces (EAFs) produce about 29% of worldwide steel, of which most is produced from recycled material. This recycling process generates enormous amounts of electric arc furnace dust (EAFD). It is estimated that a tonne of molten metal produces about 11-20 kg of EAFD [2, 3]. This implies that about 8-13 Mt of EAFD is generated annually. This dust is considered a secondary source for zinc, it contains 7-40 % zinc depending on the proportion of galvanized steel scrap recycled [2, 4]. Therefore, zinc recovery from EAFD is of prime importance in terms of energy efficiency and resource conservation. The only industrial process currently employed for zinc recovery from EAFD is the Waelz Kiln process. This technology is applied in 30-35 locations across the world in order to recycle about 45% of EAFD [5]. The attempts to use alternative technologies for recycling EAFD such as hydrometallurgical methods have failed so far due to technical, environmental or economic constraints.

Recently, recycling EAFD combined with plastic waste has been a thematic research topic with a number of recently reported studies. This technology utilizes the presence of halogens in plastics, such as chlorides in PVC and bromides in brominated flame retardant materials (BFRs) to react with the metal oxides present in the EAFD. Upon decomposition of these plastics, the corresponding hydrogen halides of (HCl or HBr) are released, converting metal oxides into chlorides or bromides at moderate temperatures (below 573 K (300 ^{o}C)). Metal halides formed can be either heated further to evaporate them [4, 6-9], or leached with water from the pyrolysis residue as demonstrated in recent studies [10-13].

Understanding the interaction between the EAFD and PVC/BFRs is important for process development, especially the thermodynamics of pyrolysis. To the authors best knowledge, literature provides no account of the thermodynamics underpinning the pyrolysis of EAFD-BFR/TBBPA mixtures, although, one can find several publications on the interaction between metal oxides or EAFD with TBBPA [4, 8, 9, 12, 14-16]. Likewise, quantum chemical calculations have mapped out reaction pathways between Fe_2O_3 (a minor constituent in EAFD) with products from thermal decomposition of TBBPA [17].

TBBPA is considered as one of the most important feed materials for the manufacture of flame retardants. It has been used in printed circuit boards, insulated wires and various polycarbonate plastics for many years to improve the fire safety of such products. TBBPA accounts for approximately half of all BFRs in production today due to high efficiency and compatibility with most types of polymers [18]. Due to the enormous growth in the global electronics industry and the very short life span of electronics, electronic materials become obsolete quickly, which causes an accumulation of electrical wastes causing significant issues concerning their safe disposal and recycling of these types of materials.

The most common method for the treatment of waste brominated flame retardants (BFRs) is pyrolytic incineration. To reduce the release of HBr during incineration of materials laden with BFR, it is recommended to mix BFRs with metal oxides. To this end, this paper has two aims; firstly to investigate the thermal behavior of EAFD-TBBPA mixtures during pyrolysis experimentally through both TGA and isothermal pyrolysis, and secondly to present thermodynamic calculations pertinent to the reactions between HBr and selected prominent metal oxides present in the dust.

2. Materials and methods

The chemical composition of EAFD was analyzed by using a Perkin Elmer Optima 700 inductively coupled plasma atomic emission spectrometer (ICP-AES) after representative samples of the dust were microwave digested according to the method developed by Al-Harahsheh *et al* [19]. This method was slightly modified to dissolve all of the dust sample. The mineralogical composition of the collected EAFD sample was characterized by X-Ray diffraction analysis technique (XRD) as reported in Al-Harahsheh *et al* [13].

Powdered 4,4′-isopropylidenebis(2,6-dibromophenol), a commercial brominated flame retardant commonly referred to as 3,3′,5,5′-tetrabromobisphenol-A, (TBBPA), was purchased from Sigma-Aldrich. It was mixed with EAFD, collected from a Jordanian steel smelter located at Hashimia- Jordan, at 1:1 and 1:3 mass ratios of EAFD: TBBPA, these mixtures were designated as E-TBBPA1, and E-TBBPA3, respectively.

Thermogravimetric and differential scanning calorimetry (DSC) analyses of the initial materials (EAFD, TBBPA) and their mixtures were performed using a TA-Q600 thermal analyzer. A representative 10 mg sample of the specified material was placed in a platinum pan and heated at 5 and 10 ^{0}C/min under nitrogen with a flow rate of 50 ml/min.

Chemical thermodynamics calculations were performed using the software “Facility for the Analysis of Chemical Thermodynamics (FactSage)” [20]. FactSage implements the free Gibbs enthalpy minimization method [21], to calculate the concentrations of chemical species when the specified compounds react partially or totally to reach a state of chemical equilibrium. The calculations were performed for the two mixtures (E-TBBPA1 and E-TBBPA3) in order to find the concentrations of all product species at different temperatures and to compare the results

with the analogous experimental values obtained in this study. Furthermore, the Gibbs free energy was calculated for the proposed reactions at different temperatures in order to elucidate the thermodynamic feasibility of each reaction to take place.

The pyrolysis of the EAFD-TBBPA mixtures was performed according to the procedure reported elsewhere [13], whereby, pellets of the mixture were placed inside a U-shaped Pyrex tube between two layers of quartz wool. The pellets were heated in a programmable Nabertherm® furnace at a specified heating rate and were then held at a final temperature for 30 minutes, while purging with high purity nitrogen. The pyrolysis residue was characterized by XRD to identify the crystalline reaction products.

3. Results and discussion

3.1. Chemical and mineralogical composition of EAFD and its residues

Table 1 shows the average elemental composition of the EAFD sample. The analysis indicated the dust contained Zn, Fe, Ca, Na, Pb, Si, K and Mn. Elements of Na and K were mainly found in the chloride form. The chloride content of the EAFD was found to amount to 8.32± 0.15 % as determined by silver nitrate titration [22]. The carbon content of the sample was analyzed by calorimetry and was found to be 2.63 ± 0.03 % with 0.11± 0.01 % being inorganic carbon, which implies the presence of about 1 % of carbonates in the dust.

Figure 1 shows the XRD analysis of a representative EAFD sample. The peaks confirm that the dust consists mainly of zincite (ZnO), franklinite ($ZnFe_2O_4$), magnetite (Fe_3O_4), halite (NaCl),

sylvite (KCl), lead hydroxyl chloride (PbOHCl) and hematite (Fe_2O_3). It is possible also that the dust may contain a hydrated zinc chloride such as semonkolleite.

Figure 1 also shows The XRD pattern of the pyrolysis residue treated at a temperature of 623 K (350 ^oC) for 30 minutes; the major phases present are magnetite/franklinite, $PbBr_2$, KPb_2Br_5, $K_{2P}bBr_4$, NaBr, KBr, K_2ZnBr_4 and sphalerite. However, $ZnBr_2$ and $FeBr_2$ were not seen in the sample as these most were likely to be in an amorphous form. Water leaching test performed on this residue resulted in dissolution of all of the lead (100 %), 82.5 % Zn, and 38.1 % Fe. The residue after leaching was found to contain mainly magnetite and some silicates, most probably iron silicates.

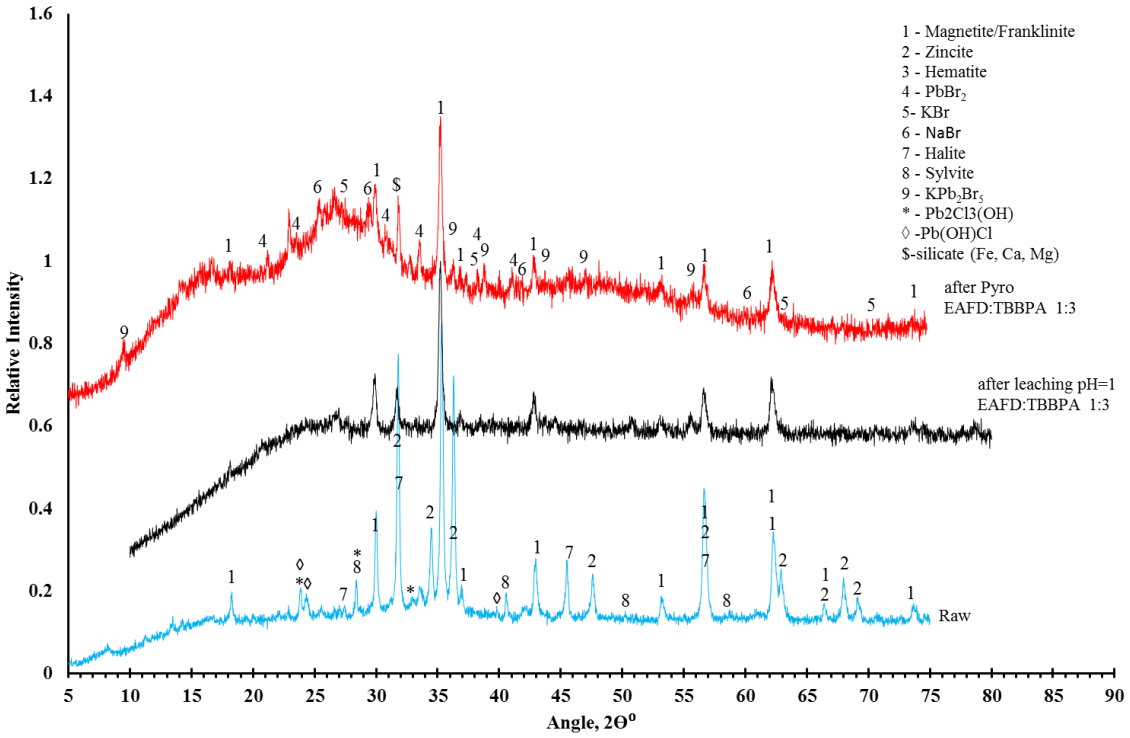

Figure 1 XRD pattern of raw EAFD, E-TBBPA3 after pyrolysis and after leaching at pH=1

3.2. TGA and DTA analyses

3.2.1. TGA and DTA analysis of EAFD-TBBPA mixtures

Thermogravimetric analysis (TGA) under an inert atmosphere (N_2) was performed for pure TBBPA and for E-TBBPA1 and E-TBBPA3 mixtures containing 50, and 25 % of EAFD, respectively. Figure 2 presents a comparison of the pyrolysis behavior of E-TBBPA1 and E-TBBPA3 under inert conditions, at a heating rate of 10 °C/min. At a ratio of 1:1 the decomposition of TBBPA seems to start at a lower temperature (~ 458 K (185 °C)) than the sample in the ratio 1:3 where more TBBPA is present. At a temperature of 453 K (180 °C), TBBPA melts as seen in the DTA profile presented in Figure 4. Reactions occurring in the condensed medium upon melting of TBBPA are most likely to be dominated by successive C-Br bond sessions and cross-linking reactions. On the other hand, decomposition of pure TBBPA in the gas phase was shown to commence with fission of a C-CH_3 bond [23].

The other distinctive feature of the TGA profile of E-TBBPA1 (Figure 3) is the weight loss peak, the maximum of which corresponds to a temperature of about 1088 K (815 °C). Thermodynamic analysis using FactSage software (see section 3.3.2.2), suggests that a reduction in non-volatile iron compounds into iron and evaporation of $FeBr_2$ starts intensively at temperatures above 943 K (670 °C). Of course the delay observed here is related to the non-isothermal nature of the TGA experiment and also the direct reduction of iron oxide by solid carbon according to reaction 9 shown below. When the TBBPA content increases in the mixture, the weight loss peak at 1088 K (815 °C) is not observed in the TGA profile (E-TBBPA3), because there will be no iron oxide left for reduction by carbon, as all of the iron available has

been consumed in the bromination reaction. This becomes evident when inspecting the DTA profile shown in Figure 4 (see also section 3.3.2.2).

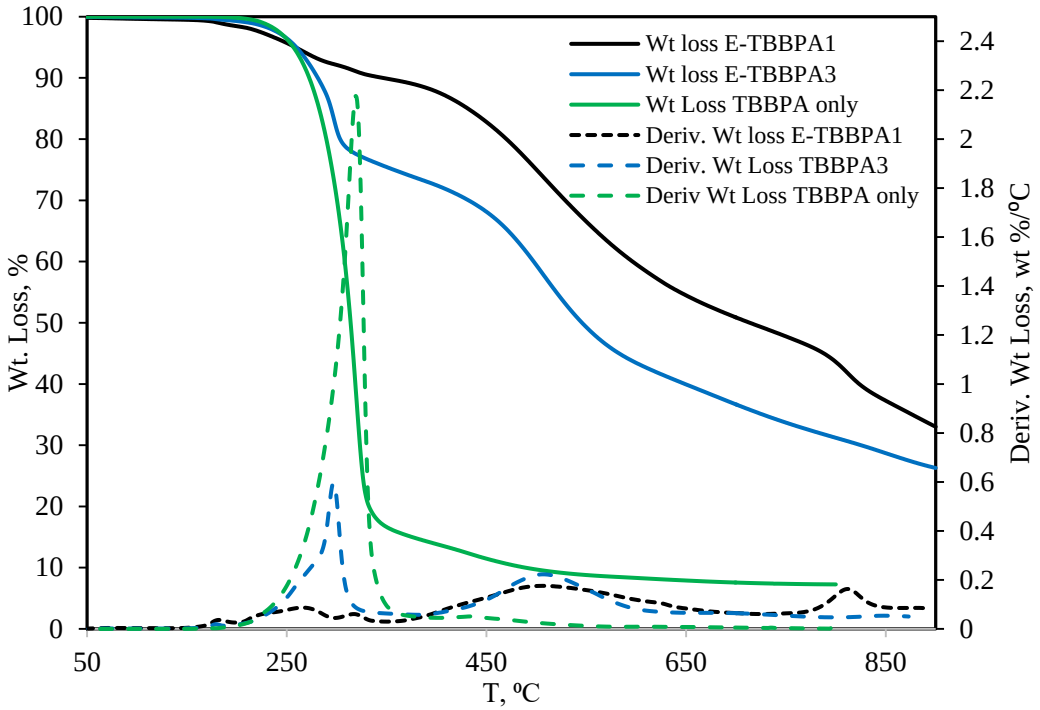

Figure 2 TGA and DTG profiles for pure TBBPA, E-TBBPA1 and E-TBBPA3 at a heating rate of 10 ^{0}C/min.

Figure 3 shows weight loss and derivative weight loss for E-TBBPA1 and E-TBBPA3 mixtures at heating rates of 5 and 10 °C/min. Several events seem to occur during the thermal pyrolysis of the mixtures; the slow heating rates and the high proportion of dust display more features of the interaction between EAFD and TBBPA. The weight loss of the first event, when E-TBBPA1 was pyrolyzed, is observed at a temperature of about 453 K (180 °C) (see Figure 3a), which coincides with the melting point of TBBPA. This suggests that a reaction between EAFD and liquid TBBPA occurs as the peak of this event is shifted to the right with an increase in the heating rate. Oleszek *et al* [16] observed a weight loss in this temperature region when TBBPA was pyrolyzed with PbO. They managed to detect water by TGA-MS across this temperature

region. Based on this, it is likely that the solid-liquid reaction between metal oxides present in the dust (most likely ZnO and PbO) and TBBPA may occur at this temperature leading to the formation of metal bromides and the release of water vapor (Reactions 4 and 6). Grabda *et al* [14] came to similar conclusions when they studied the de-bromination of TBBPA by ZnO. Al-Harahsheh *et al* [13] also detected some metal bromides when they leached a TBBPA-EAFD pyrolysis residue pyrolysed at temperatures below 523 K (250 °C). Likewise, it has been shown theoretically that the successive dissociative addition of HBr over Fe-O entities to result in the formation of direct iron bromide precursors accompanied with the evolution of water via facile reaction barriers [23].

At a heating rate of 5 °C/min, three successive and partially overlapped events seem to occur with maxima at temperatures of 495, 524 and 581 K (222, 251 and 308 °C). These maxima are shifted to 516, 537 and 589 K (243, 264 and 316 °C), respectively at a heating rate of 10 °C/min. The peaks marked 2, 3 and 4 (Figure 3a) could be related to evaporation of TBBPA, evaporation of its decomposition products (like phenols and bromophenols) and bromination of metal oxides, respectively [16]. The derivative mass loss peaks 5 at 733 K (460°C) may be assigned to the evaporation of zinc bromide (see section 3.3.2.1). The TGA analysis for several metal bromides performed by Oleszek et al [15, 16] suggests the following order of metal bromide evaporation: $ZnBr_2$ (~ 643- 733 K (370-460 °C)), $PbBr_2$ (~ 723 – 803 K (450-530 °C)) and then $FeBr_2$ (~ 793- 943 K (520-670 °C)).

Peak 6 at a temperature of 875 K (602 °C) may be assigned to the reduction of hematite to wustite, which is further reduced to metallic iron by char starting from 1023 K (750 °C) (at 5

°C/min) and peaks at 1068 K (795 °C) (peak 7). Iron transformation from its oxides to metallic iron can be presented in the following sequence:

Fe_3O_4 ➔ FeO ➔ Fe

In a recent study by Al-Harahsheh *et al* [12], both FeO and Fe were detected in the residue after microwave treatment of EAFD-TBBPA mixtures.

The derivative weight loss peak 8 (Figure 3a) occurring at a temperature of 1123 K (850 °C) and at a heating rate of 5 °C/min are related to the evaporation of NaBr, KBr $FeBr_2$, $MnBr_2$, metallic zinc as shown in Figures 6-11.

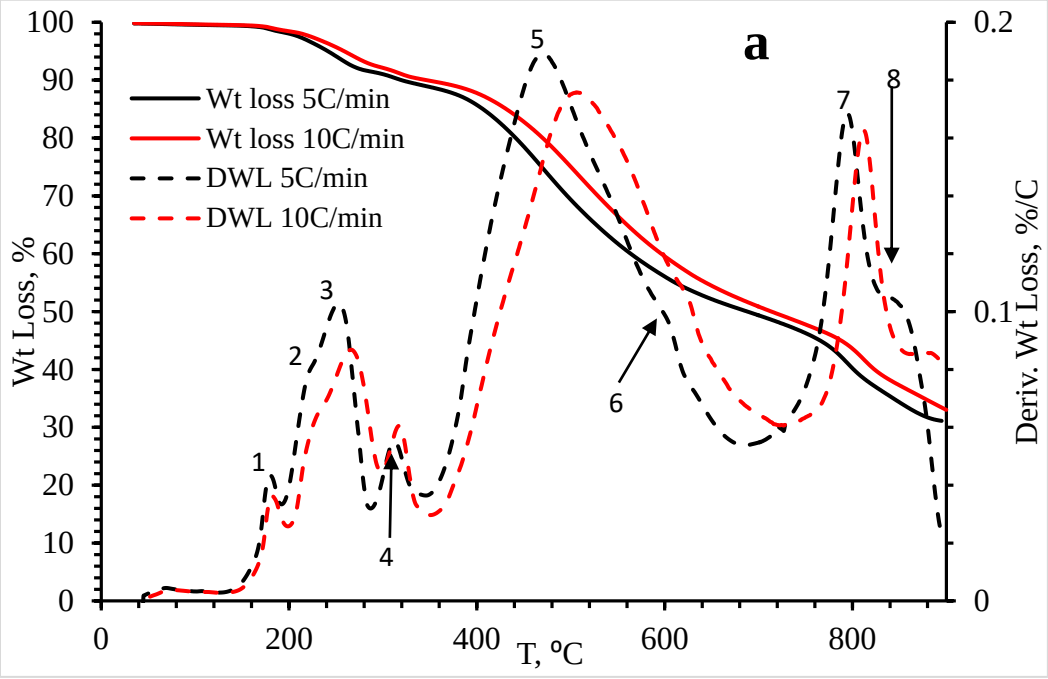

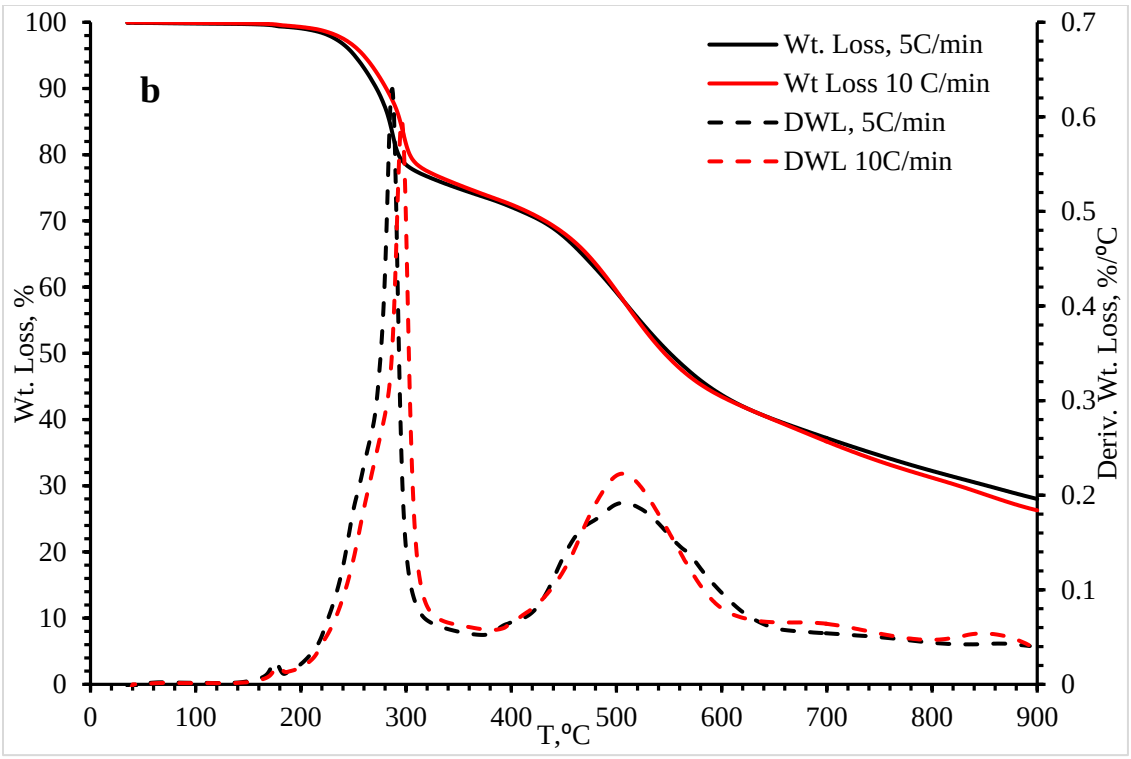

Figure 3 Weight loss and weight loss derivative for E-TBBPA1 (a) and E-TBBPA3 (b) at heating rates of 5 and 10°C/min

Thermal analysis shows that pure TBBPA exhibited two endothermic events (Figure 4); the first one is a sharp peak at a temperature of 453 K (180 °C) which represents the melting of TBBPA, while the second event is a broad peak (533-623 K (260-350 °C)) with a maxima at 602 K (329 °C) representing thermal decomposition of TBBPA. When EAFD was mixed with TBBPA, the first endothermic event (smelting of TBBPA) appeared in the same place irrespective of the EAFD: TBBPA ratio. This endothermic event is also accompanied by a small weight loss as discussed above. However, the second event is now exothermic and shifted to the left. The maxima appears now at 592 and 574 K (319, and 301 °C) for E-TBBPA1, and E-TBBPA3, respectively. Detailed observation of this exothermic event, especially for E-TBBPA1, suggests two successive events occurring at 591 and 673 K (319 and 400 °C) for E-TBBPA1. These

exothermic phenomena are marks the formation of metal bromides such as $ZnBr_2$, $FeBr_2$, NaBr, KBr and $PbBr_2$ as a result of the bromination reactions of metal oxides present in the dust by HBr as well as formation of iron silicate (Fe_2SiO_4). The exothermic nature of the metal oxide bromination into metal bromides has also been confirmed via quantum chemical calculations. For instance, dissociation of HBr over Fe-O bond was found to be exothermic by 227.6 kJ/mol (54.4 kcal/mol) [23].

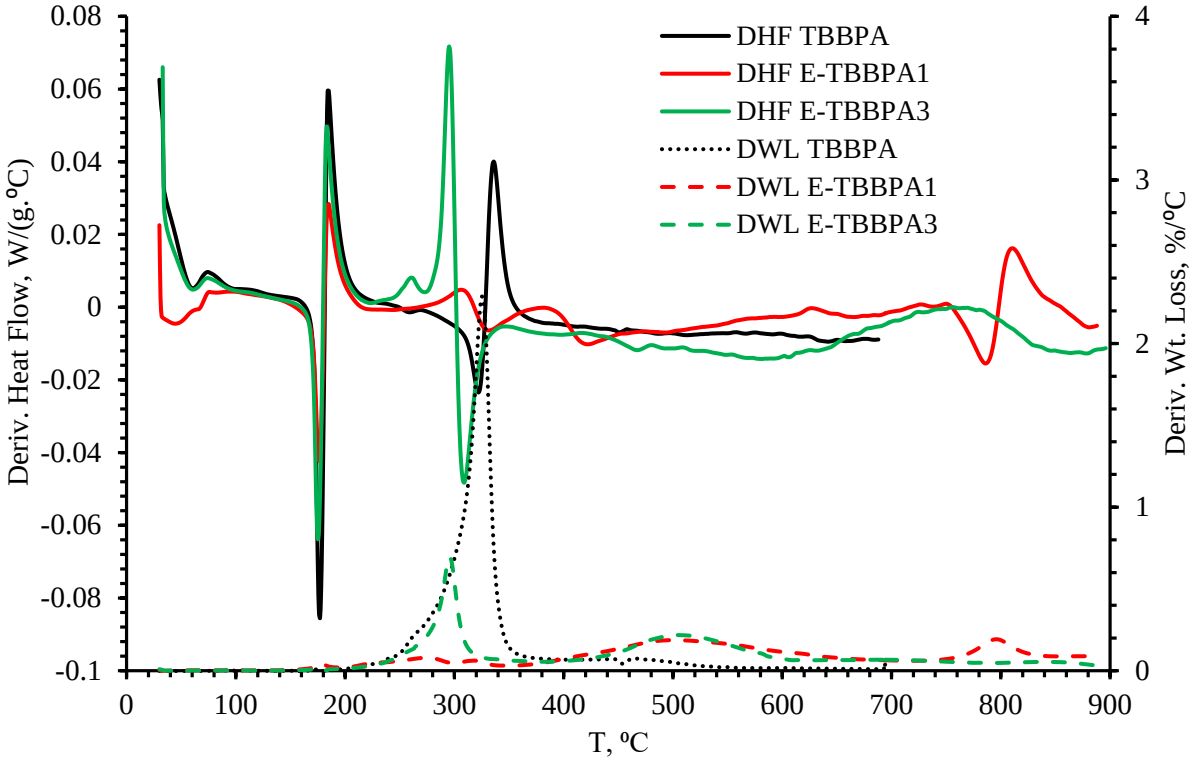

Figure 4 Heat flow derivatives for pure TBBPA, E-TBBPA1 and E-TBBPA3 mixtures obtained at a heating rate of 10 °C/min (DWL-Derivative weight loss, DHF-Derivative heat flow).

The endothermic event observed in the heat profile of E-TBBPA1 at about 1073 K (800 °C) is consistent with the weight loss observed in the TGA profile of the same mixture which may be related to the evaporation of NaBr, KBr, $FeBr_2$, $MnBr_2$, and metallic zinc.

3.3. Chemical thermodynamic calculations

The mineral composition of the EAFD was calculated based on the types of minerals obtained from XRD analyses as well as on the elemental analysis using ICP-AES. The estimated composition of the minerals in the EAFD is presented in Table 2. When calculating the mineral composition, it was assumed that 50 % zinc present in the dust is in the form of franklinite and the remaining exists as zincite. For iron, it was assumed that the remaining iron after calculating the franklinite content was 80 % in the form of magnetite while 20 % is in the form of hematite.

These mineral phases will undergo through several main reactions according to the list shown below [6]:

$$Fe_2O_3(s) + 6\ HBr(g) \rightarrow 2FeBr_3(s,l,g) + 3H_2O\ (g) \quad (1)$$

$$ZnFe_2O_4 + 8HBr \rightarrow ZnBr_2 + 2FeBr_3(g) + 4H_2O \quad (2)$$

$$Fe_3O_4(s) + 2HBr(g) \rightarrow FeBr_2(s,l) + Fe_2O_3(s) + H_2O(g) \quad (3)$$

$$PbO(s) + 2HBr\ (g) \rightarrow PbBr_2(s,l) + H_2O\ (g) \quad (4)$$

$$CaO(s) + 2HBr\ (g) \rightarrow CaBr_2\ (s,l) + H_2O(g) \quad (5)$$

$$ZnO(s) + 2HBr(g) \rightarrow ZnBr_2(s,l) + H_2O(g) \quad (6)$$

$$ZnFe_2O_4(s) + 2HBr(g) \rightarrow ZnBr_2(s,l) + Fe_2O_3(s) + H_2O(g) \quad (7)$$

$$PbOHCl + 2HBr \rightarrow PbBr_2 + H_2O + HCl \quad (8)$$

$$2Fe_2O_3 + 3\ C \rightarrow 4Fe + 3\ CO_2 \quad (9)$$

3.3.1. Gibbs free energy

Gibbs free energies for the above reactions were calculated using FactSage® software version 7.0 across the temperature range 273 to 1273 K (0 to 1000 °C) with a step of 10 °C. Figure 5 shows the results of the thermodynamic calculations for the above reactions. Based on the thermodynamic spontaneous scale (i.e., $\Delta G_r < 0$), it becomes evident that all reactions can proceed at all temperatures commencing from room temperature to 1273 K (1000 °C) except for Reactions 1, 2, 3 and 9. Reaction 1, bromination of hematite, can only take place at a temperature below 593 K (320 °C), while Reaction 2, or bromination of franklinite, can only take place at a temperature below 733 K (460 °C). On the other hand, Reaction 3, bromination of magnetite, can take place at temperature below 1033 K (760 °C). Reaction 9, reduction of hematite, can only take place at temperature above 873 K (600 °C)

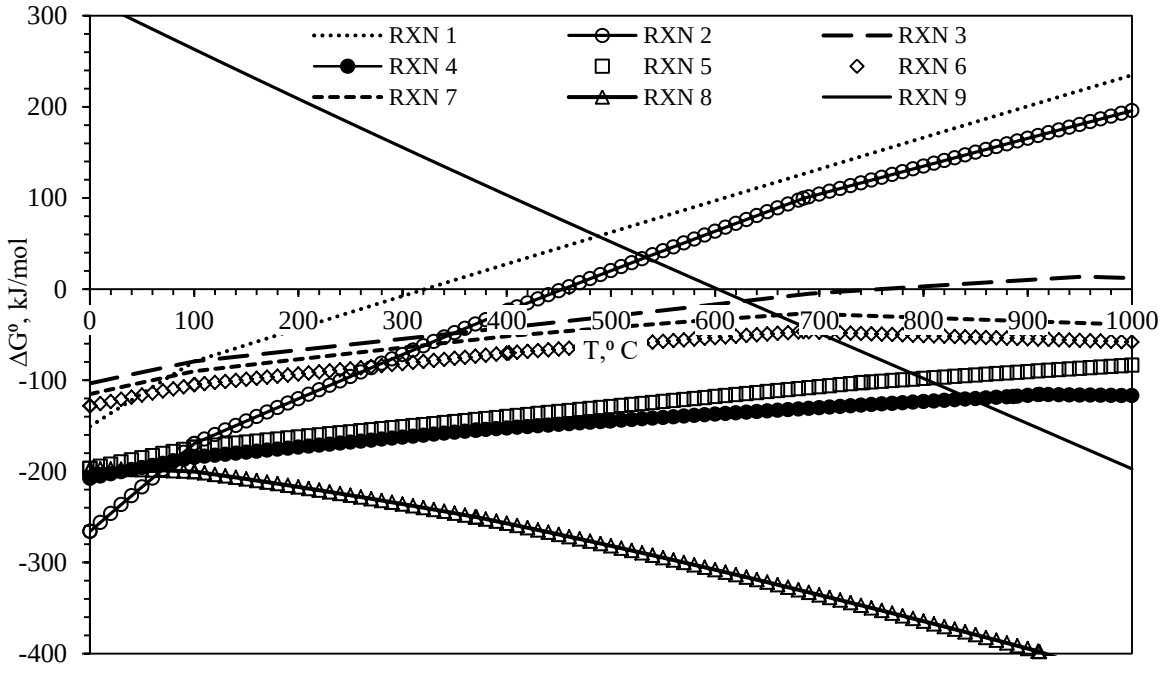

*Figure 5 Gibbs free energy for the suggested reactions (**RXN 1 to RXN 9**).*

3.3.2. Chemical equilibrium calculations

Chemical equilibrium calculations were also performed using FactSage® for E-TBBPA1 and E-TBBPA3 assuming that the initial mass of the mixture was 100 g. It is important to point out that the TBBPA content in the mixture was replaced by its theoretical content of HBr in these thermodynamic calculations. Additionally, carbon was assumed to form during thermal decomposition of TBBPA, therefore, based on the TGA profiles of the mixtures of these ratios, a fixed amount of carbon was assumed to be present in the mixture .The calculations were performed across the temperature 473 to 1173 K (200 to 900 °C) with a step of 10 °C. The initial temperature was assumed to be 473 K (200 °C) based on the fact that at 493 K (220 °C) HBr is released from the mixture during pyrolysis as indicated earlier (Figure 2). Phases formed at concentrations below 0.01 g were ignored.

The results of the thermodynamic simulations are shown in Figures 6 to 11; each of which presents the results of both considered ratios. It was found that at least 200 species were formed in different proportions over the considered temperature range. For the purpose of simplicity the obtained results for the different species formed were grouped into zinc (Figure 6), iron (Figure 7) and lead (Figure 8) compounds, bromide gases (Figure 9), sodium (Figure 10), potassium (Figure 11) and other compounds (Appendix 1).

3.3.2.1. Behavior of zinc

Figure 6 shows the expected zinc compounds formed during the course of pyrolysis of E-TBBPA1 and E-TBBPA3 mixtures. As anticipated the major phase seen is $ZnBr_2$, which is immediately formed upon the release of HBr. It melts at about 683 K (410 °C), where it also starts to evaporate reaching completion at about 883 K (610 °C). This result is consistent with

the weight loss observed in the TGA profile of the E-TBBPA1 indicated by peak 5 (Figure 3). The two other major phases formed are sphalerite (ZnS) and zinc aluminate ($ZnAl_2O_4$), these phases seem to form in very small quantities in the case of E-TBBPA3. Willemite (Zn_2SiO_4) forms in very small quantities and it peaks in the temperature region between 843 and 873 K (570 and 600 °C). Such a phase was detected in the pyrolysis residue of E-TBBPA1 as reported by Al-Harahsheh *et al* [12]. Sphalerite was also detected in the pyrolysis residue of E-TBBPA3 as seen in the XRD pattern shown in Figure 1. Willemite formed in E-TBBPA1 seems to react with metal chlorides (KCl and NaCl) at temperatures above 873 K (600 °C) to form zinc chloride ($ZnCl_2$), $NaZnCl_3$ and $KZnCl_3$ gases. The quantity of which is minimal for the sample at a ratio of 1:3 due to the low proportion of willemite. Sphalerite remains stable over the whole temperature region studied, whereas, zinc aluminate ($ZnAl_2O_4$) starts to decompose at temperatures above 973 K (700 °C), whereby part of its zinc reacts with the HBr to form zinc bromide gas (see Figure 6a) while the other part reduced to zinc by the carbon formed into zinc gas. For the sample at a ratio of 1:3, the sphalerite reacts with HBr to produce zinc bromide and H_2S gases, the later reacts with a fraction of wustite (FeO) forming iron sulphide ($FeS_{(s)}$) (see Figure 7b).

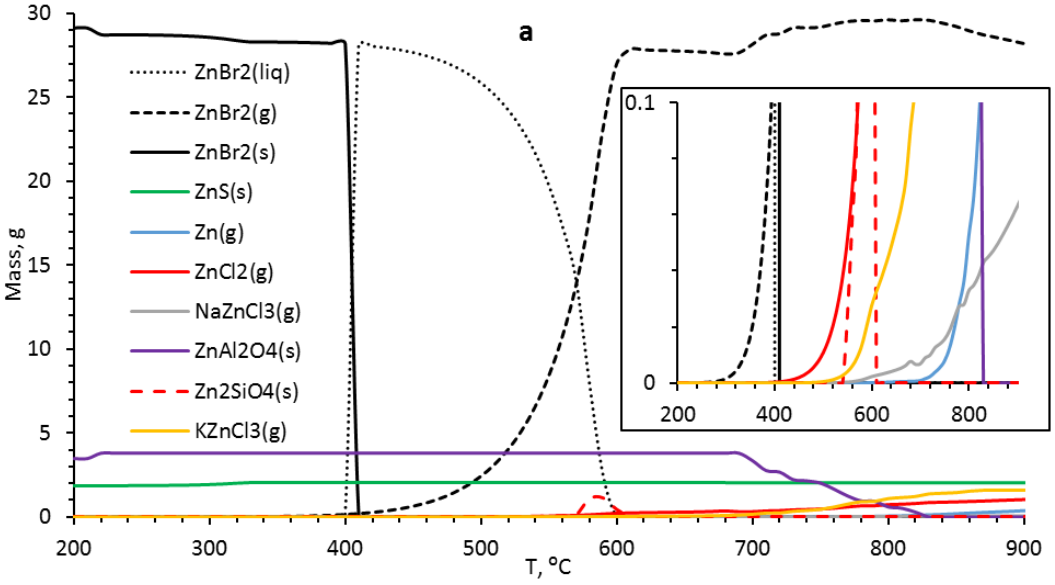

285

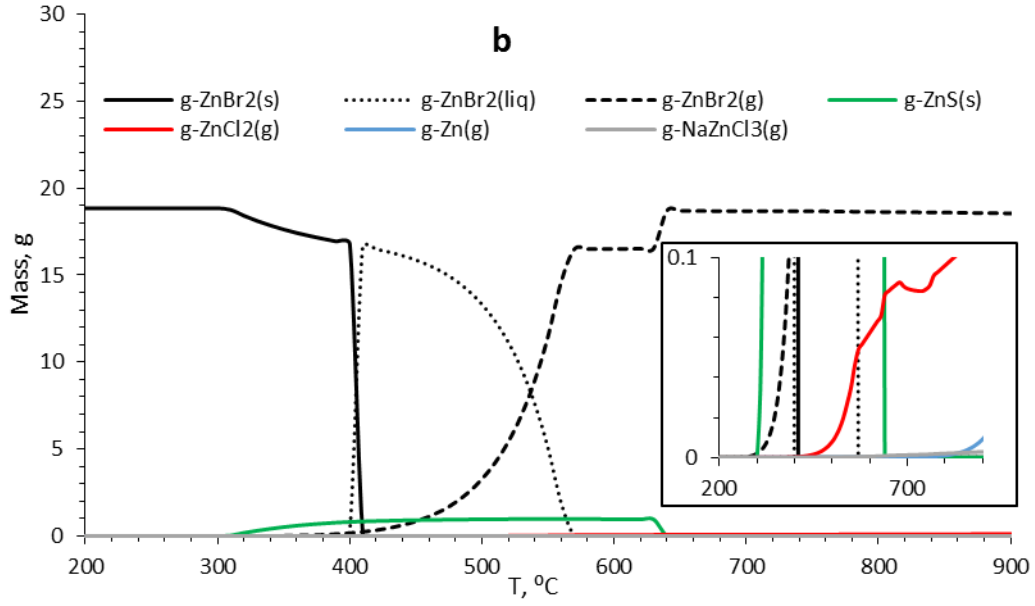

286

287 ***Figure 6 Thermodynamic calculations for zinc compounds of E-TBBPA1 (a) and E-TBBPA3 (b)***

288 ### 3.3.2.2. Behavior of Iron

289 Figure 7 shows the expected iron compounds formed during the course of pyrolysis of E-
290 TBBPA1 and E-TBBPA3 mixtures. The major phase present in the E-TBBPA1 pyrolysis residue
291 is magnetite. The quantity of the latter is almost double that in the feed mixture. This suggests

292 that the iron in franklinite was converted into magnetite, while zinc in franklinite has converted
293 into $ZnBr_2$. The magnetite phase is reduced into wustite (FeO) at a temperature of 620 °C then
294 into iron (Fe) at a temperature of 943 K (670 °C) followed by further transformation into
295 cementite (Fe_3C) at 1093 K (820 °C) due to the presence of carbon from the TBBPA skeleton.
296 These events can be clearly observed in DTG and DTA profiles for E-TBBPA1 as presented in
297 Figure 4 (see Appendix 1 for the details of TGA-DTA profile of E-TBBPA1). Zhang *et al* [24]
298 studied earlier the carbothermic reduction of iron oxides in EAFD and obtained similar results.

299 Small quantities of solid $FeBr_2$ were seen to form across the temperature region 473 and 573 K
300 (200 and 300 °C), and seem to react with silica to form iron silicate (see their mirror profile in
301 Figure 7a). This behavior has direct implications for the selective separation of zinc bromide
302 from the pyrolysis residue of E-TBBPA mixtures by water leaching as observed by Al-
303 Harahsheh *et al* [13], where iron dissolution was substantially reduced from the residue
304 pyrolysed at 723 K (450 °C).

305 The origin of solid $FeBr_2$ must result from the reaction between magnetite and HBr according to
306 reaction 3 or from $FeBr_3$ formed according to reactions 1 and 2. The latter is an unstable gas and
307 readily decomposes into $FeBr_{2(s)}$ and Br_2 gas according to the following reaction [13, 16].

308 $$FeBr_{3(s)} \xrightarrow{>473\ K} FeBr_{2(s)} + Br_{2(g)} \qquad (10)$$

309 $FeBr_2$ reforms again in the gas form at temperature of 873 K (600 °C), most likely, from the
310 reaction between wustite and HBr (see HBr profile in Appendix 1). Iron silicate (Fe_2SiO_4) and
311 calcium iron silicates ($Ca_3Fe_2Si_3O_{12}$) are formed in the temperature region from 553 to about 983
312 K (280 to about 710 °C), which then decomposes back into SiO_2 and FeO. Across the
313 temperature region from 863 to 1003 K (590 to 730 °C), iron silicate reacts with calcium

bromide and chloride to form $Ca_2FeSi_2O_7$, which then decomposes into Fe and other calcium silicates (see Appendix 1). Additionally, part of the iron oxide participates in the reaction with TiO_2 across the temperature region from 473 up to 1013 K (200 up to 740 °C), and also decomposes back into Fe and TiO_2, where the later forms other Ca - titanates and Ca-Ti silicates.

With an abundance of HBr in the E-TBBPA3, the behavior of iron is distinct from that of E-TBBPA1. Almost all iron from the magnetite, franklinite and hematite is now in the form of solid $FeBr_2$ which starts to sublimate at a temperature of 863 K (590 °C) and then smelting occurs co-currently from 973 K (700 °C). It exists completely in gas form as from 1033 K (760 °C). Above a temperature of 903 K (630 °C), small quantities of the other iron phases are formed such as FeS, $CaFeSi_2O_6$, $FeCl_2$, and $KFeCl_{3\ (g)}$ (Figure 7b). Neither Fe nor Fe_3C were formed with the sample in the ratio 1:3 due to the absence of sufficient quantities of iron oxides, that were initially completely converted into iron bromides

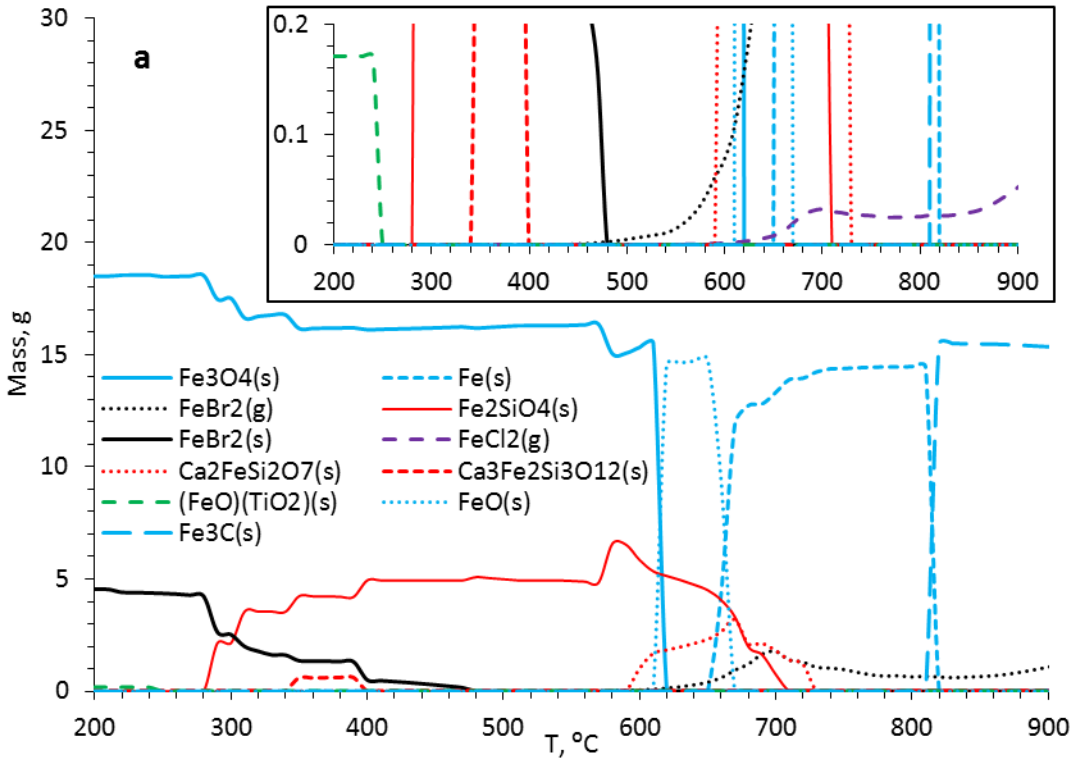

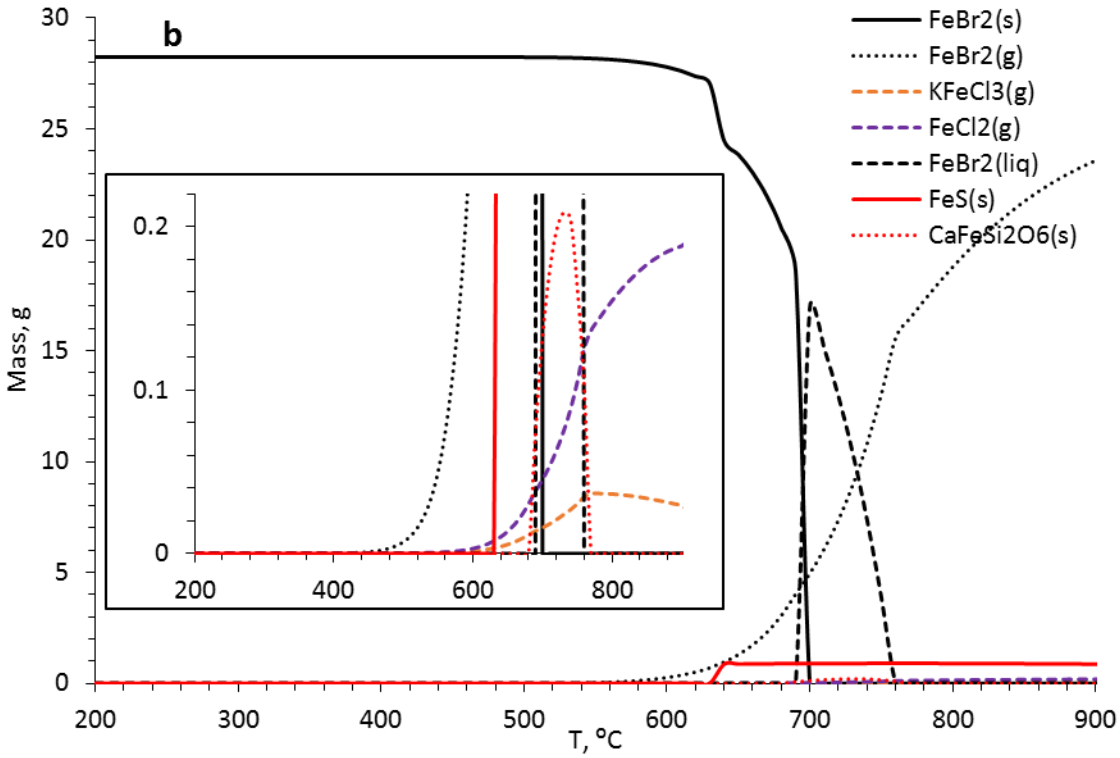

*Figure 7 Thermodynamic calculations for iron compounds of E-TBBPA1 (**a**) and E-TBBPA3 (**b**).*

The major difference in the behavior of iron in EAFD in presence of different proportions of TBBPA imposes significant implications for the separation of zinc and lead, in bromide form, from EAFD, leaving iron in its oxide form. Tuning the EAFD-TBBPA mixture composition and the pyrolysis temperature may lead to complete separation of lead and zinc bromides either in gas form [4, 25] or by leaching with water [13]. Grabda *et al* [4] have managed to recover as high as 82 % Zn and 20 %Pb from EAFD when pyrolyzed, in 20vol % O_2+80vol % Ar atmosphere, with TBBPA at a ratio of 1:3 and at a temperature of 823 K (550 ^{o}C). Apparently, the high TBBPA content has led to formation of iron bromides that react partially with oxygen to form iron oxides. The current thermodynamic and TGA study suggests that working under inert atmosphere with lower TBBPA content would lead to formation of only zinc and lead bromides leaving iron in the oxide form. In support to this, Al-Harahsheh *et al* [13] have managed to

recover about 91 % Zn and almost 100 % Pb from a EAFD-TBBPA mixture, pyrolysed at a temperature of 623 K (350 °C), by leaching of the pyrolysis residue in water solution.

3.3.2.3. Behavior of lead

Figure 8 shows the expected lead compounds formed during the course of pyrolysis of E-TBBPA1 and E-TBBPA3 mixtures. The major lead phase seen, in both ratios, is solid $PbBr_2$ which appears to exist as from 473 K (200 °C) in quantities equivalent to the Pb content in the dust. Lead bromide smelts at a temperature of 653 K (380 °C) and completely evaporates at a temperature of 883 K (610 °C). Traces of other lead compound gases are formed at temperatures above 773 K (500 °C). The results of thermodynamic calculations agree with the experimental data reported by Al-Harahsheh *et al* [13] in which the pyrolysis residue of E-TBBPA2, $PbBr_2$ was found to form based on XRD analysis and SEM observation reported therein.

Oleszek *et al* [26] studied the thermal degradation of TBBPA in the presence of lead oxide under inert conditions. They found that bromination by lead oxide proceeds simultaneously with the thermal decomposition of TBBPA leading to the formation of $PbBr_2$. The $PbBr_2$ volatilization began at 588 K (315 °C), increased at 1023 K (750 °C), and reached a maximum (98 %) at a temperature of 1123 K (850 °C). The carbon in the residue reduced the unreacted lead oxide to metallic lead across the range 588- 1023 K (315–750 °C).

The thermodynamic results shown in Figure 8 reveal that, the formation of gaseous metallic lead started at a temperature of 1023 K (750 °C), mainly in the case of E-TBBPA1 where a deficient amount of HBr is expected for bromination reactions. Nevertheless, the quantity of metallic lead formed here as well as the other reduced species (PbBr and PbCl) seem to have formed as a

result of degradation of $PbBr_2$ seen in Figure 8b, and not due to the reaction of unreacted lead oxides with carbon residues. Figure 5 shows that the most thermodynamically preferable reaction was the reaction between lead oxychloride and HBr.

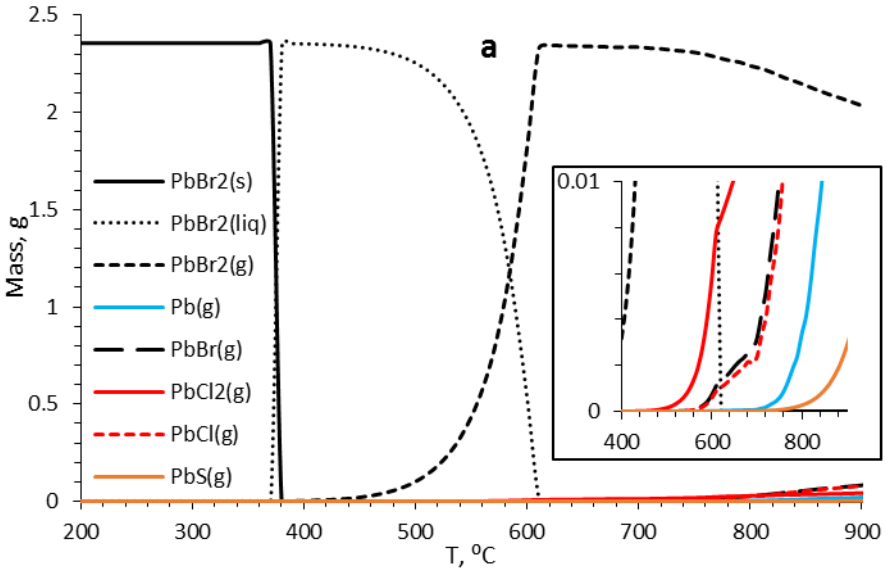

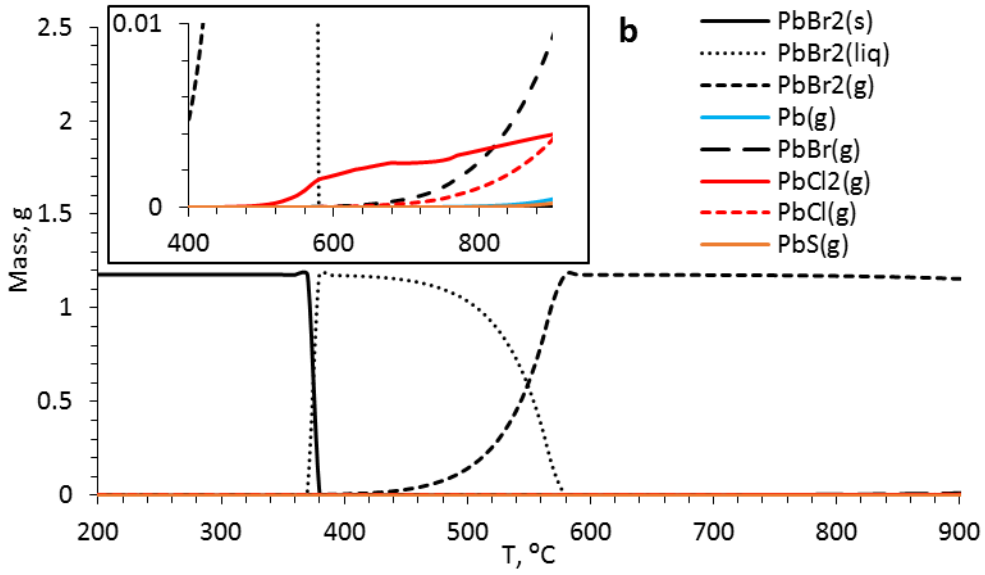

Figure 8 Thermodynamic calculations for lead compounds of E-TBBPA1 (a) and E-TBBPA3 (b).

3.3.2.4. Formation of metal bromide gases

Figure 10 shows the bromide gases expected to form during the course of pyrolysis of E-TBBPA1 and E-TBBPA3 mixtures. The major bromide gas formed during pyrolysis of the E-TBBPA1 mixture is $ZnBr_2$ which starts to evolve at a temperature of about 593 K (320 ^{0}C). The metal bromides present in the EAFD emerge according to the following sequence: $CuBr_3$, $ZnBr_2$, $PbBr_2$, $FeBr_2$, $MnBr_2$, KBr, NaBr, $CaBr_2$ and finally $MgBr_2$. This order is independent on the amount of TBBPA present in the mixture. This sequence has great implication for the possibility of separating these bromides based on their boiling points.

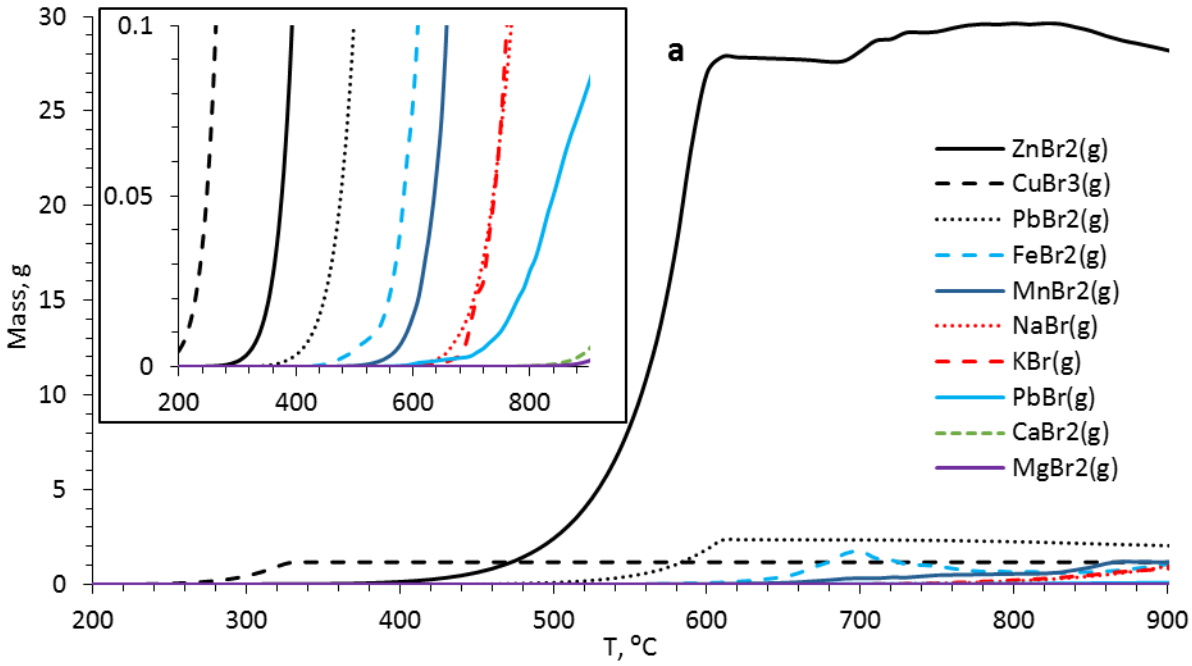

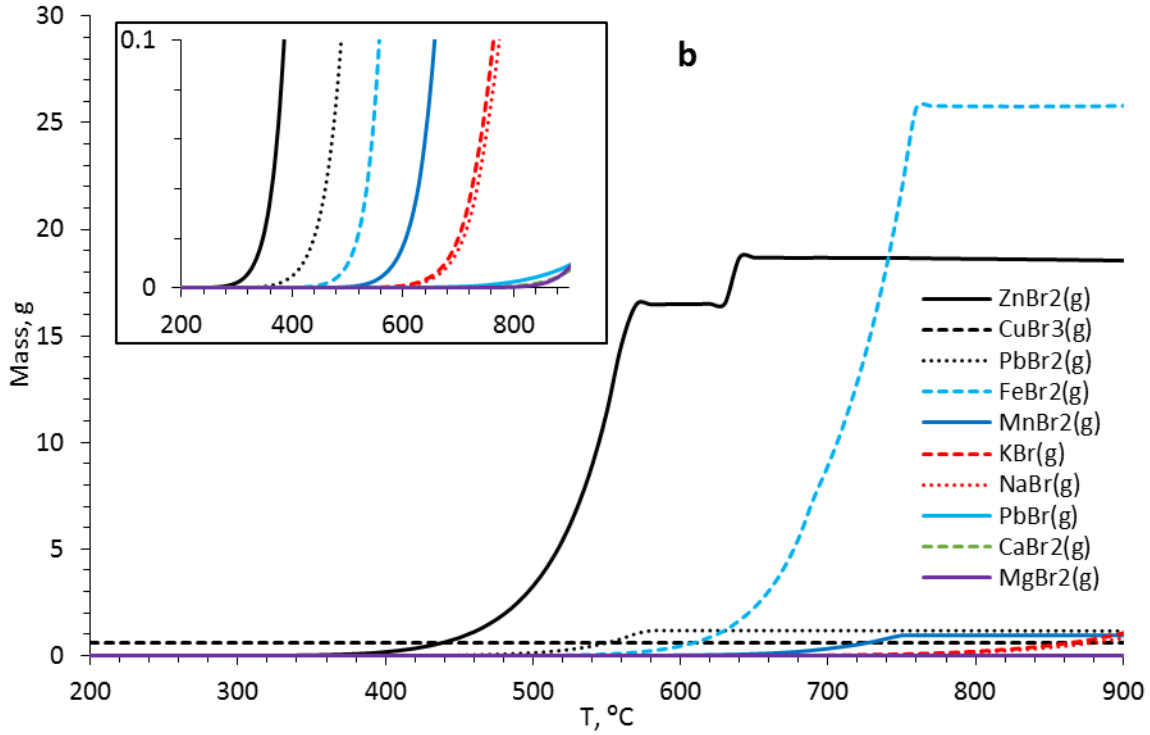

*Figure 9 Thermodynamic calculations for bromide gases formed during pyrolysis of E-TBBPA1 (**a**) and E-TBBPA3 (**b**).*

3.3.2.5. Effect of presence of NaCl and KCl salts in EAFD

The EAFD used in this work, as seen in Table 2, contains about 7 % NaCl and 3 %KCl; the presence of these salts certainly affects the thermodynamics of E-TBBPA mixtures. As demonstrated in Figure 10, sodium bromide consumes appreciable quantities of the HBr available from TBBPA, while chloride from the initial salts tends to form double salts such as $NaMnCl_3$ and $NaZnCl_3$ at temperatures above 823 K (550 °C). Sodium bromide smelts at about 1023 K (750 °C).

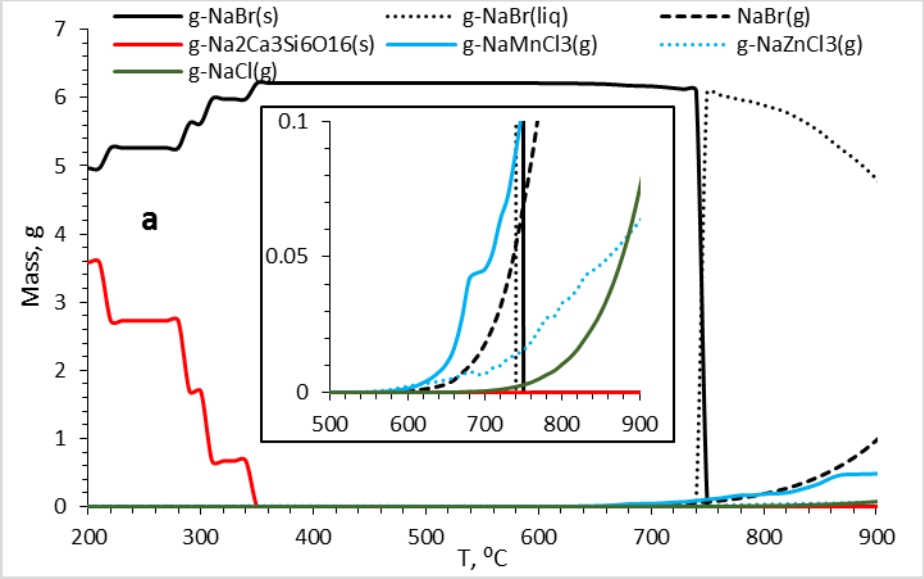

387

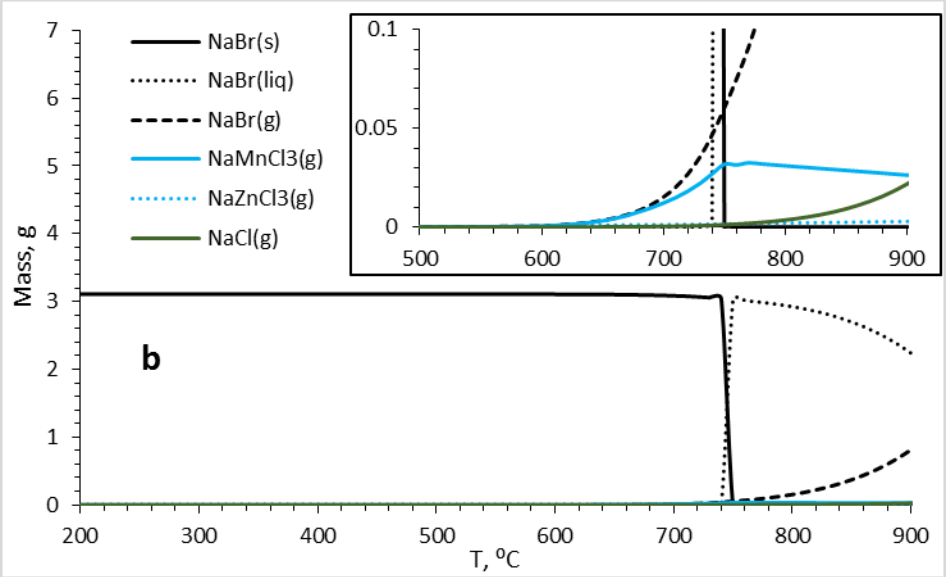

388

389 ***Figure 10 Thermodynamic calculations for sodium compounds formed during pyrolysis of E-TBBPA1***

390 ***(a) and E-TBBPA3 (b)***

391 Potassium, forms double chloride salts ($KCaCl_3$ and $KMnCl_3$) at low temperatures for ratio 1:1,

392 while other double chloride salts are formed at temperatures above 823 K (550 ^{0}C). Potassium

393 bromide, in both liquid and solid forms, appears only at temperatures above 1023 K (750 ^{0}C) for

the sample in ratio 1:1. However, at E-TBBPA ratio 1:3 KBr forms at significantly lower temperatures.

For the purpose of selective separation between iron, lead and zinc, it may be suggested that these salts are washed prior to pyrolysis for three reasons; to increase the concentration of Zn, Pb and Fe in the dust, to reduce the quantity of HBr needed for bromination of metal oxides present in the dust and finally to inhibit the formation of metal chlorides which would provide better selective separation.

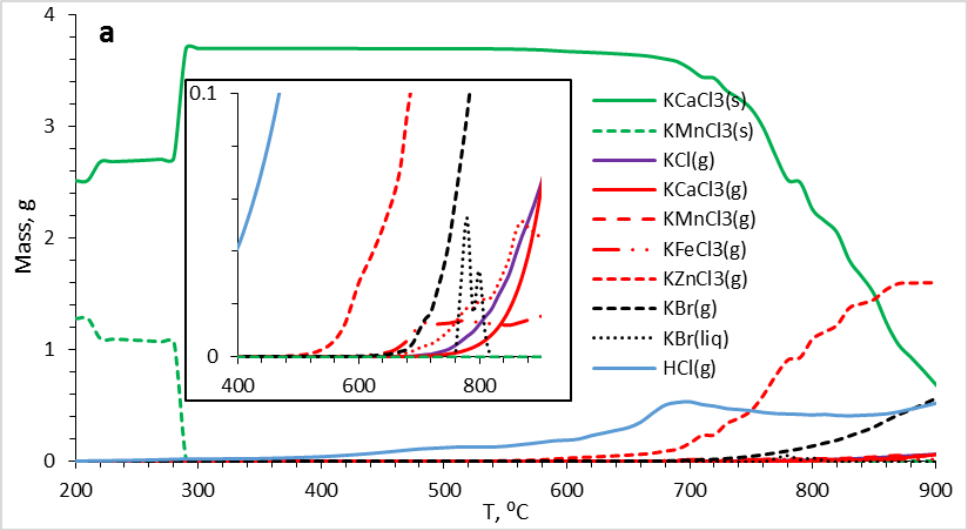

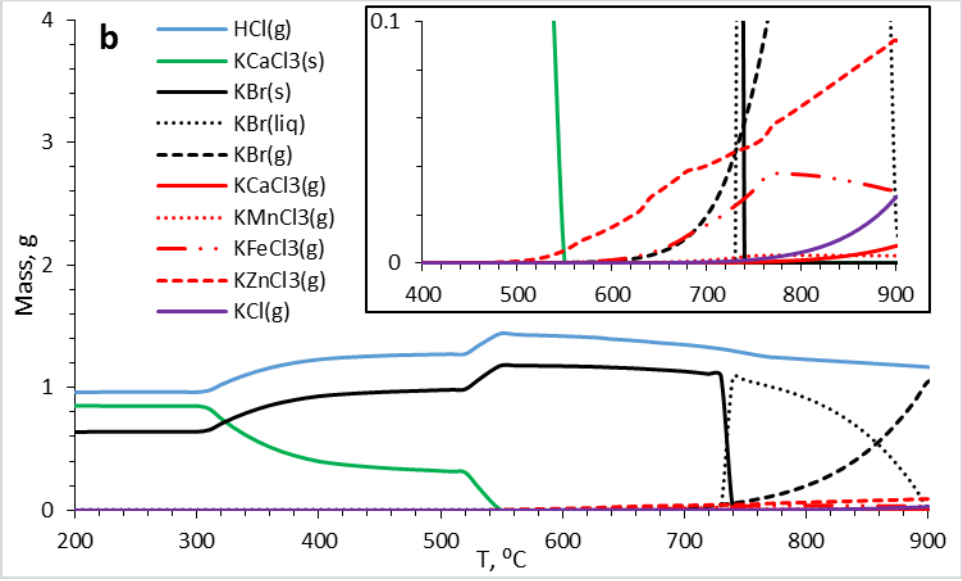

Figure 11 Thermodynamic calculations for potasium compounds formed during pyrolysis of E-TBBPA1 (a) and E-TBBPA3 (b)

4. Conclusions

The thermal pyrolysis and thermodynamic behavior of EAFD-TBBPA mixtures were studied in this work across a temperature region from room temperature up to 1073 K (1000 °C). The degradation of these mixtures proceeded through several steps including the melting of TBBPA followed by the release of HBr from TBBP, which reacted with the metal oxides present in the EAFD to form metal bromides. These bromides, upon further heating evaporated at different temperatures. This facilitates their selective evaporation according to the following sequence: $CuBr_3$, $ZnBr_2$, $PbBr_2$, $FeBr_2$, $MnBr_2$, KBr, NaBr, $CaBr_2$ and finally $MgBr_2$. Thermodynamically, it was found that the least preferable bromination reactions are those involving iron compounds including hematite, magnetite and franklinite. Lead bromination was the most thermodynamically preferable reaction. Thermodynamic calculations also suggest that tuning the quantity of TBBPA would lead to preferential bromination of lead and zinc in favor of iron. As a consequence, lead and zinc bromides can be selectively separated from iron at moderate temperatures by evaporation, while char formed by the degradation of TBBPA may be successfully used as a reducing agent for iron oxides into metallic iron.

5. Acknowledgment

The authors would like to thank the deanship of scientific research at Jordan University of Science and Technology (projects: 104/2014 and 137/2016) for financing this work.

6. References

[1]. WSA, "Resource efficiency" (World Steel Association, 2016), https://www.worldsteel.org/steel-by-topic/sustainable-steel/environmental/efficient-use.html, Accessed 15/09/2016.

[2]. Oustadakis P, Tsakiridis P E, Katsiapi A, and Agatzini-Leonardou S, *J. Hazard. Mater.* 2010, vol. 179, pp. 1-7.

[3]. Liebman M. *Recycling of Metals and Engineered Materials*. 2013, John Wiley & Sons, Inc., pp. 237-250.

[4]. Grabda M, Oleszek S, Shibata E, and Nakamura T, *J. Hazard. Mater.* 2014, vol. 278, pp. 25-33.

[5]. Antrekowitsch J, Rösler G, and Steinacker S, *CHEM-ING-TECH* 2015, vol. 87, pp. 1498–1503.

[6]. Lee G S and Song Y J, *Miner Eng* 2007, vol. 20, pp. 739-746.

[7]. Tailoka F and Fray D J. *EPD Congress*, TMS, 1997, pp. 475-93

[8]. Grabda M, Oleszek S, Shibata E, and Nakamura T, *J. Hazard. Mater.* 2011, vol. 187, pp. 473-479.

[9]. Liu G-B, Zhao H-Y, and Thiemann T, *J. Hazard. Mater.* 2009, vol. 169, pp. 1150-1153.

[10]. Al-Harahsheh M, Al-Otoom A, Al-Makhadmah L, Hamilton I E, Kingman S, Al-Asheh S, and Hararah M A, *J. Hazard. Mater.* 2015, vol. 299, pp. 425-436.

[11]. Al-Harahsheh M, Kingman S, Al-Makhadmah L, and Hamilton I E, *J. Hazard. Mater.* 2014, vol. 274, pp. 87-97.

[12]. Al-Harahsheh M, Kingman S, and Hamilton I E, *J Anal Appl Pyrol* 2017, vol. Accepted.

[13]. Al-Harahsheh M, Aljarrah M, Rummanah F, Abdellateef K, and Kingman S, *J Anal Appl Pyrol* 2017, vol. 125, pp. 50-60.

[14]. Grabda M, Oleszek S, Shibata E, and Nakamura T, *Environ Sci Technol* 2009, vol. 43, pp. 8936-8941.

[15]. Oleszek S, Grabda M, Shibata E, and Nakamura T, *Thermochim Acta* 2012, vol. 527, pp. 13-21.

[16]. Oleszek S, Grabda M, Shibata E, and Nakamura T, *Thermochim Acta* 2013, vol. 566, pp. 218-225.

[17]. Altarawneh M, Ahmed O H, Jiang Z T, and Dlugogorski B Z, *J. Phys. Chem. A* 2016, vol. 120, pp. 6039-6047.

[18]. Marongiu A, Bozzano G, Dente M, Ranzi E, and Faravelli T, *J Anal Appl Pyrol* 2007, vol. 80, pp. 325-345.

[19]. Al-Harahsheh M, Kingman S, Somerfield C, and Ababneh F, *Anal Chem Acta* 2009, vol. 638, pp. 101-105.

[20]. FactSage, "FactSage 7.1" (GTT-Technologies, 2016), http://www.factsage.com/, Accessed 15/10/2016.

[21]. Bale C W, Chartrand P, Degterov S A, Eriksson G, Hack K, Ben Mahfoud R, Melançon J, Pelton A D, and Petersen S, *Calphad* 2002, vol. 26, pp. 189-228.

[22]. DIN. *DIN EN 196 - 2 Methods of testing cement – Part 2: Chemical analysis of cement*. 2005.

[23]. Altarawneh M and Dlugogorski B Z, *J. Phys. Chem. A* 2014, vol. 118, pp. 9338-9346.

[24]. Zhang H, Li J, Xu A, Yang Q, He D, and Tian N, *J Iron Steel Res Int* 2014, vol. 21, pp. 427-432.

[25]. Terakado O, Ohhashi R, and Hirasawa M, *J Anal Appl Pyrol* 2011, vol. 91, pp. 303-309.

[26]. Oleszek S, Grabda M, Shibata E, and Nakamura T, *J. Hazard. Mater.* 2013, vol. 261, pp. 163-171.

463 Table 1. Chemical composition of EAF dust obtained from ICP-AES analysis (dry base wt.%)

Zn	Fe	Ca	Na	Pb	Si	K
25.91±0.09	18.04±0.31	3.98±0.03	3.29±0.03	3.15±0.03	2.76±0.08	1.84±0.02
Mn	S	Mg	Al	Cu	Sn	Ti
1.24±0.01	0.78±0.01	0.64±0.01	0.50±0.00	0.29±0.01	0.172±0.003	0.128±0.004
Cr	Cd	Ni	Bi	V	Co	
0.015±0.007	0.039±0.001	0.025±0.003	0.007±0.000	0.003±0.000	0.002±0.000	

464

465 Table 2 Estimated mineral composition of the EAFD.

compound	Wt%	compound	Wt%
$ZnFe_2O_4$	40.4	SiO_2	5.0
ZnO	13.6	KCl	3.0
Fe_3O_4	11.7	MnO_2	1.7
Fe_2O_3	3.0	MgO	0.7
$CaCO_3$	4.2	Cu_2O	0.6
$CaSO_4$	5.7	TiO_2	0.2
NaCl	7.1	Al_2O_3	0.4
PbO	2.9		

466

467

Figures captions

Figure 1 XRD pattern of raw EAFD, E-TBBPA3 after pyrolysis and after leaching at pH=1

Figure 2 TGA and DTG profiles for pure TBBPA, E-TBBPA1 and E-TBBPA3 at a heating rate of 10^0C/min.

Figure 3 Weight loss and weight loss derivative for E-TBBPA1 (A) and E-TBBPA3 (B) at heating rates of 5 and 10^0C/min

Figure 4 Heat flow derivatives (B) for pure TBBPA, E-TBBPA1 and E-TBBPA3 mixtures obtained at a heating rate of 10 ^{0}C/min (DWL-Derivative weight loss, DHF-Derivative heat flow).

Figure 5 Gibbs free energy for the suggested reactions (RXN 1 to RXN 9).

Figure 6 Thermodynamic calculations for zinc compounds of E-TBBPA1 (a) and E-TBBPA3 (b)

Figure 7 Thermodynamic calculations for iron compounds of E-TBBPA1 (a) and E-TBBPA3 (b)

Figure 8 Thermodynamic calculations for lead compounds of E-TBBPA1 (a) and E-TBBPA3 (b)

Figure 9 Thermodynamic calculations for bromide gases formed during pyrolysis of E-TBBPA1 (a) and E-TBBPA3 (b).

Figure 10 Thermodynamic calculations for sodium compounds formed during pyrolysis of E-TBBPA1 (a) and E-TBBPA3 (b)

Figure 11 Thermodynamic calculations for potasium compounds formed during pyrolysis of E-TBBPA1 (a) and E-TBBPA3 (b)

Appendix 1

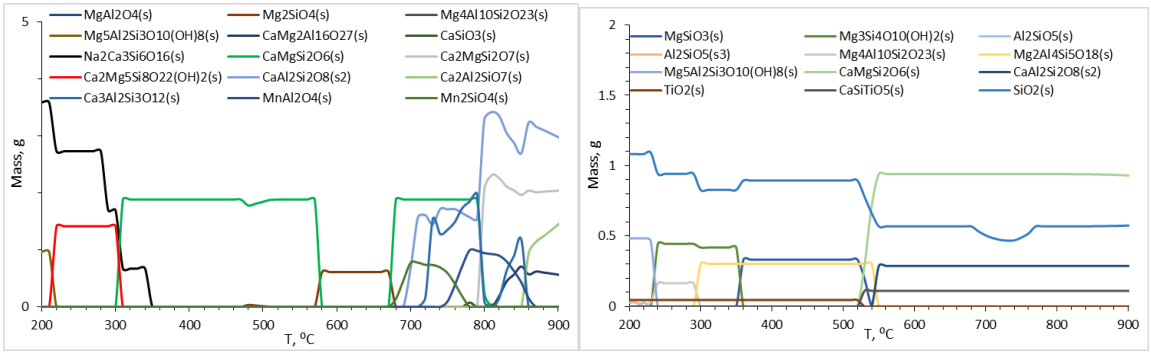

Figure A1 Thermodynamic calculations for silicates of E-TBBPA1 (Left pannel) and E-TBBPA3 (right panel)

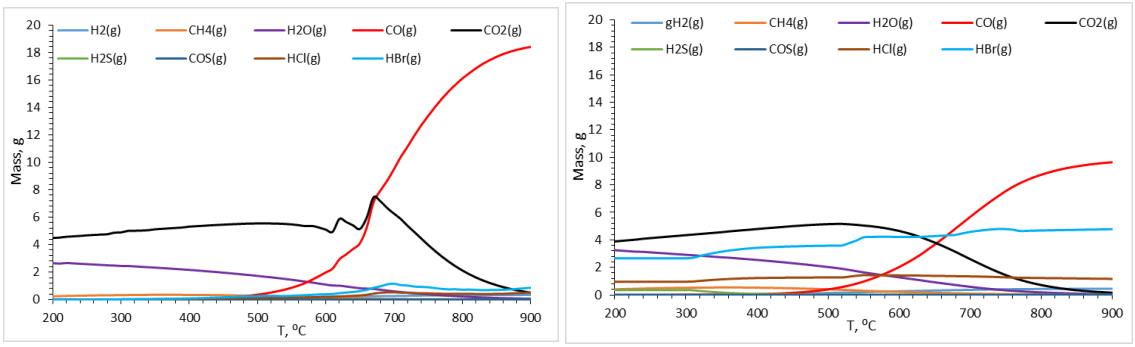

Figure A2 Thermodynamic calculations for non condensable gases of E-TBBPA1 (Left pannel) and E-TBBPA3 (right panel)

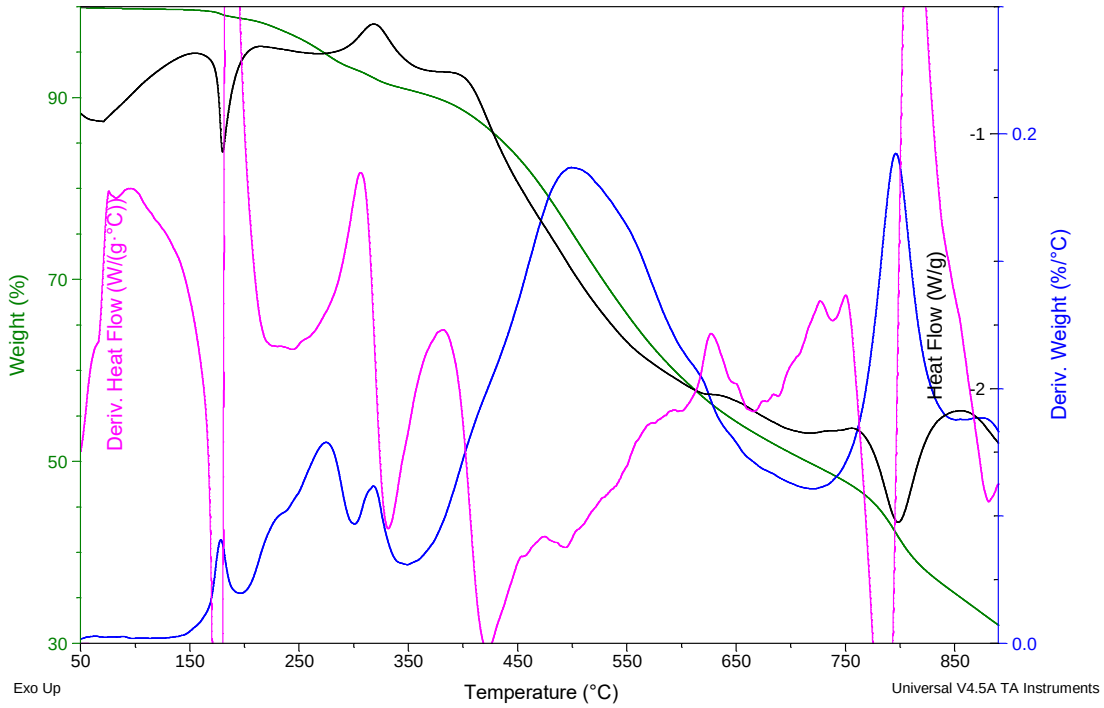

Figure A3. TGA-DTA profile for E-TBBPA1